Earth Surf. Dynam. Discuss., 1, 387–405, 2013
www.earth-surf-dynam-discuss.net/1/387/2013/
doi:10.5194/esurfd-1-387-2013

Earth Surface Dynamics
Discussions
Open Access

Generalized swath profiles

S. Hergarten[1], **J. Robl**[2], **and K. Stüwe**[3]

[1]Universität Freiburg i. Br., Institut für Geo- und Umweltnaturwissenschaften, Freiburg i. Br., Germany
[2]Universität Salzburg, Institut für Geographie und Geologie, Salzburg, Austria
[3]Universität Graz, Institut für Erdwissenschaften, Graz, Austria

Received: 22 August 2013 – Accepted: 4 September 2013 – Published: 16 September 2013

Correspondence to: S. Hergarten (stefan.hergarten@geologie.uni-freiburg.de)

Published by Copernicus Publications on behalf of the European Geosciences Union.

Abstract

We present a new method to extend the widely used geomorphic technique of swath profiles towards curved structures such as river valleys. The basic idea consists in using the oriented distance from a given baseline (e.g., a valley floor) as the profile coordinate. The method can be implemented easily and avoids almost all problems related to alternative ideas of generalizing the concept of swath profiles. Some examples of the application to valleys, a large subduction zone, and an impact crater are provided in order to illustrate the capabilities of the method.

1 Introduction

Swath profiles are a widespread tool to eliminate small-scale structures from topographic profiles. In principle, computing a swath profile is nothing else but stacking several parallel profiles. As illustrated in Fig. 1, computing a swath profile involves extending the original profile line (green) to a rectangle of a given width (the swath; black), and the elevation data are stacked along red lines normal to the profile line. In this context, stacking concerns computing at least a mean value of the elevations along the red lines, but in many cases, minimum and maximum values or the standard deviation are determined and analyzed, too.

Considering wider swaths leads to smoother profiles, i.e., removes small-scale topographic structures and thus helps to recognize the main topographic shape. But in return, swath profiles are subject to a systematic bias as soon as the topography contains curved structures such as river valleys. Profiles across valleys are among the most widely used types of topographic profiles. Even if the original profile line is normal to the baseline (e.g., the valley floor), stacking along the red lines in Fig. 1 loses track of the baseline depending on its curvature. As a consequence, even a perfectly V-shaped valley will look more like a U-shaped valley where the width of the artificially flattened valley floor increases with the curvature of the valley and the width of the swath.

Swath profiles have been used in numerous geomorphic studies (e.g., Fielding et al., 1994; Montgomery, 2001; Reiners et al., 2003; Mitchell and Montgomery, 2006a, b; Rehak et al., 2008; Robl et al., 2008). As mentioned by Grohmann (2004), the basic idea even dates back to the 1920s. The implementation in Geographic Information Systems has been addressed in several online tutorials and discussions and, e.g., by Grohmann (2004). Theoretical aspects were considered by Telbisz et al. (2012). In this paper it was already mentioned that swath profiles are in principle not restricted to rectangular swaths, but also allow the consideration of curved structures. As an example, the application of "central swath profiles" where the profile coordinate is the distance from a given point to the morphology of a volcano was presented.

As an ordinary swath profile is nothing else but stacking parallel topographic profiles, one could think of extending swath profiles towards arbitrary curved baselines by stacking several non-parallel profiles where each of them is normal to the baseline at different points on the baseline. The green lines in Fig. 2 illustrate this concept. Provided that the origin of each individual profile line is located at its intersection with the baseline, this method avoids the systematic bias due to the curvature of the baseline. However, this method still suffers from some problems. First, the density of the individual profiles varies within the considered domain, so that points close to the center of the baseline's curvature contribute more to the resulting swath profile than regions at the other side. It is also easily recognized in Fig. 2 that the same surface point may even contribute to several of the stacked profiles, but at different profile coordinates. As a second problem, this method requires some smoothing of the baseline (e.g., if it is an automatically derived valley floor) since the orientation of the individual profile lines is very sensitive to the small-scale roughness of the baseline.

Although all these problems may not be crucial, getting around them requires at least a considerable technical effort. We therefore present a new method avoiding these problems.

ESURFD
1, 387–405, 2013

2 The new method

Our approach refrains from defining individual profiles, but directly uses the oriented distance of any surface point from the baseline instead. In this context, oriented distance shall mean that all points to the right-hand side of the baseline have a positive distance, while those to the left-hand side have a negative distance. This oriented distance defines the position of the considered surface point on the resulting generalized swath profile. In principle, this method stacks the elevation data along the red lines of constant oriented distance in Fig. 2.

Computing these lines of constant distance would, of course, be rather demanding. However, we do not need these lines explicitly, but simply travel along the entire domain instead, i.e., along all points of the DEM (digital elevation model) in the discrete case. We therefore only need to compute the oriented distance of each DEM point towards the baseline of the profile, which is discussed in the next section more in detail.

Apart from the advantage of its simplicity, this procedure guarantees that each DEM point contributes exactly once to the profile, and it is robust against the roughness of the baseline. It is easily recognized that the lines of small distances follow this roughness, those of larger distances become smooth.

In return, the obtained distances are arbitrary numbers and are not restricted to discrete values as it would be the case for ordinary swath profiles parallel to one of the coordinate axes. Therefore, transferring the distances and elevations to a profile requires binning. The bin width defines the spatial resolution of the resulting profile.

Some care should be devoted to the selection of the domain that is taken into account if the baseline is given. This domain is obviously limited by the desired length of the profile, but the end point should be explicitly taken into account. Without further constraints, the lines of constant distances would be ovals in case of a straight baseline, but the curved edges of these ovals are obviously not within the scope of our idea and may introduce a strong bias, e.g., in case of profiles across valleys. The easiest way to get around this problem is to consider only these surface points where

ESURFD

1, 387–405, 2013

the closest point on the baseline is neither the starting point nor the end point of the baseline. The red lines in Fig. 2 already take this constraint into account.

3 Implementation

The implementation of our method based on a DEM and a baseline defined by a polygonal line is in principle straightforward. In a first step, a tight rectangle parallel to the coordinate axes around the baseline is computed. This rectangle is extended by half the length of the desired profile in each direction, so that it includes all points of the surface which may contribute to the profile. This rectangle is illustrated in Fig. 2 by the black frame.

Then, all DEM points in this rectangle are iterated, and the oriented distance of each point from the polygonal baseline is computed. As long as the number of line segments of the baseline is not too high, this can be done individually for each DEM point $\boldsymbol{p}$ without using further information. Let $\boldsymbol{b}_1, \ldots, \boldsymbol{b}_n$ be the points defining the baseline. We then determine the distance of $\boldsymbol{p}$ towards each segment, i. e., we determine λ_i for each segment $i = 1, \ldots, n-1$ in such a way that the distance between the point

$$\boldsymbol{q}_i = (1 - \lambda_i)\boldsymbol{b}_i + \lambda_i \boldsymbol{b}_{i+1} \tag{1}$$

and $\boldsymbol{p}$ is minimal under the side condition $0 \leq \lambda_i \leq 1$. The minimum of all obtained distances yields the distance of the point $\boldsymbol{p}$ to the baseline. Instead of distances, oriented distances can be computed throughout the procedure. In this case, the absolute values of the oriented distances must be considered in the minimization.

The obtained oriented distances and the respective elevation differences are then evaluated using a binning system with a bin width according to the desired profile resolution. The restriction at the end points of the baseline is readily implemented by disregarding those DEM points where the nearest point on the baseline is either $\boldsymbol{b}_1$ or $\boldsymbol{b}_n$.

ESURFD

1, 387–405, 2013

Generalized swath profiles

S. Hergarten et al.

Practically, this algorithm is sufficient in all cases where the baseline is generated manually, so that its number of segments does not exceed some hundreds. A more efficient algorithm is only necessary in case of automatically generated baselines with a high resolution, as it occurs when flow channels derived from the DEM are considered. If the length of the baseline segments is similar to the resolution of the DEM, the numerical effort increases like the baseline length raised to the power of three (or alternatively, to the DEM resolution raised to the power of three in case of a given baseline length), so that the procedure becomes expensive in case of long baselines or high DEM resolutions.

In this case, we suggest an iterative algorithm using available information on the nearest point on the baseline from the neighborhood of the considered point $\boldsymbol{p}$. We then keep track of the index of the baseline segment which contains the presumably nearest point on the baseline for each DEM point $\boldsymbol{p}$. When searching for the baseline point nearest to $\boldsymbol{p}$, we consider the information on the nearest baseline segment in the neighborhood of $\boldsymbol{p}$. Let $s_1, \ldots, s_9$ be the indices of the segments nearest to $\boldsymbol{p}$ among $\boldsymbol{p}$ and its eight direct and diagonal neighbors. We then search for the nearest point only in the baseline interval from segment $\min\{s_1, \ldots, s_9\} - 1$ to $\max\{s_1, \ldots, s_9\} + 1$. As a consequence, only a small part of the baseline has to be searched in each step. This iteration is repeated until the results do not change any more.

In order to achieve a high efficiency and to avoid getting stuck at local minima, e.g., in case of meander-like baselines, the points of the DEM should be iterated in varying directions. A straightforward scheme would be row-wise forward, row-wise backward, column-wise forward, and then column-wise backward. Practically, only the variation between forward and backward iteration is important and provided a convergence after a few iterations in all tests that were performed.

Although the examples provided in Sect. 4 were derived from DEMs on regular lattices (either Cartesian coordinates or in longitude and latitude), the method can easily be applied to arbitrary two-dimensional point clouds without any loss of efficiency. Furthermore, it is not restricted to topographic data, but applicable to any

ESURFD
1, 387–405, 2013

two-dimensional data set, e.g., hydrological data or the distribution of elements in a mineral.

An implementation of the method is available as an online tool at http://hergarten.at/geomorphology/swathprofile.php using data from several available DEMs with almost global coverage. Furthermore, a command line tool (C++ source code without requirement of any specific libraries) can be directly obtained (free of charge) from the corresponding author.

4 Applications

In order to illustrate the new method for the construction of swath profiles, the applications presented in the following focus on topographic features that are inherently curved in plan view. Beyond the obvious application to valleys we present examples of a large subduction zone and an impact structure.

4.1 Fluvial and glacial valleys

The morphological analysis of valleys is probably the best example to illustrate the advantages of the method presented here. The cross sectional shape of river valleys is often used to infer the incision process of the valley. In particular, two end members of valley shapes are usually discerned: V-shaped valley cross sections are considered to be characteristic for actively incising streams and a fluvial erosional history (e.g., Bull, 1979), while U-shaped cross sections are interpreted in terms of glacial erosion (e.g., Bonney, 1874). However, identifying these shapes quantitatively is often nontrivial: locations appropriate for representative individual cross sections are often difficult to find, e.g., because of tributaries. And as discussed in the introduction, river valleys are typically curved so that ordinary swath profiles suffer from artefacts that may even make a V-shaped valley look like a U-shaped valley.

ESURFD
1, 387–405, 2013

In Fig. 3 we use the generalized swath profile method to characterize two valleys that are famous for their fluvial and glacial erosional history, respectively: the Grand Canyon of the Colorado River which is a typical actively incising bedrock channel (e.g., Pederson et al., 2006; Wernicke, 2011) and the glacially carved Yosemite Valley of California (Gutenberg et al., 1956).

For both generalized swath profiles the baseline was chosen along the actual course of the rivers draining the valleys. Our analysis reveals that both cross sections are qualitatively similar with a flat valley floor, steep faces, and well-marked ledges forming distinct shoulders on average. As a major difference, the profile of the Grand Canyon shows several flat portions possibly indicating a multistage incision history and the flat valley floor being 5 times narrower than in the Yosemite Valley. Comparing the generalized swath profile (b) with the map (a) proves that the flat floor in the swath profile of the Grand Canyon is indeed not an artefact of our method. However, it should be noted that an artificial widening occurs if either the width of the valley or the position of the baseline relative to the valley varies along the baseline, but this artefact is in general much smaller than the bias due to the curvature in ordinary swath profiles.

Due to the ambiguity of the Grand Canyon valley shape with regard to the V-shape of fluvial profiles and in order to illustrate the power of morphological analysis of different river segments, we have also applied our method to a much smaller stream in the Eastern Alps. The Taugl River (Fig. 4) is a tributary of the Salzach River that drains a major region of the Eastern Alps. It is known to be characterized by several segments that flow through an ancient uplifted landscape, over a knickpoint in the channel profile, and in a young incised landscape. In the headwater region (Fig. 4b, c), the average cross section of the Taugl River is perfectly V-shaped with a narrow flat valley floor and an average topographic gradient of about 0.1 at the corresponding hillslopes. The central segment (Fig. 4d, e) starts downstream of a distinct knickpoint (waterfall) and describes a narrow gorge with about 50 m high vertical faces bordering the river. Above this vertical slope segment the topographic gradient declines with increasing distance to the stream forming convex hillslopes. The third segment (Fig. 4f, g) is similar to the

ESURFD
1, 387–405, 2013

middle segment, but a planation surface on the orographic left-hand side of the river is observed, This planation surface is located about 200 m above the actual base level of the Taugl River and shows a strong glacial imprint as observed by the sculpted hillslope on the left-hand side and the persisting hillslope on the right-hand side. Assisted by the results from the swath profile analysis we suggest that the Taugl valley already existed prior to the last glaciation at the position of the actual course.

4.2 Subduction zones and related oroclines

The topographic and bathymetric expression of subduction zones often show similar characteristic features over several hundred to several thousand kilometers along strike, but different features perpendicular to these zones. Abyssal plains, forebulge and the deep sea trench are located on the subducting lower plate while the related mountain ranges are located on the upper plate. In general, these geomorphic features are located at a certain distance to the subduction zone and profiles normal to the strike of these zones are useful to characterize the morphological features. However, small-amplitude features like the elastic forebulge on the subducting plate may easily be missed because they are swamped by irregularities along strike. The construction of swath profiles is therefore an essential aid in the topographic analysis, but may be hampered by the curvature of the subduction zone.

In order to illustrate the virtue of our new method, we present a topographic characterization of the curved plate boundary between the Nazca Plate and the South American Plate (e.g., Isacks, 1988) in Fig. 5. As the subduction of the Nazca Plate is clearly related to the topographic development of the Andes (e.g., Gephardt, 1994), the bathymetry and topography perpendicular to the plate boundary should exhibit characteristic features at similar distances to the plate boundary although the age of the Nazca Plate and mechanical properties are spatially diverse (e.g., Capitanio et al., 2011). For our analysis we have chosen the deep sea trench between the two plates as the best feature to align the baseline of the general swath profile. In order to illustrate the power of our method we have chosen a baseline of more than 2000 km along strike.

ESURFD
1, 387–405, 2013

In particular, the low standard deviations of the averaged topographic features illustrate the power of the approach. Beyond this, the analysis shows that the average surface elevation of the abyssal plane of the Nazca plate is −4.3 km with a standard deviation of less than 0.5 km. Outliers are predominantly local topographic maxima and are recognized as seamounts and in case of minima graben structures. The forebulge at a distance of −50 to −100 km to the trench accounts for an average increase of about 0.2 km of surface elevation, relative to the abyssal plains. The deep sea trench is on average 6.5 km deep with a standard deviation of about 0.7 km indicating a very uniform depth distribution on the subsiding plate. On the side of the continental South American Plate, the surface elevation reaches the sea-level at a distance of about 100 km from the trench. The standard deviation is small (approximately 0.7 km), indicating a uniform active continental margin over more than 2000 km in strike of the zone. The highest average surface elevation reaches about 4 km (with peaks above 6 km) and appears at a distance of 250 km from the trench. Here the standard deviation amounts to 0.8 km going along with the variable width of the Andes with a maximum west-east extent approximately at the maximum curvature of the trench. At a distance of 250 km and beyond the average surface elevation declines, while the standard deviation (> 1 km) increases rapidly. Obviously, topography build-up is still related to the subduction of the Nazca plate, but no longer uniformly distributed in strike of the zone. In summary, the swath profile constructed with our method shows that there are indeed characteristic topographic features perpendicular to the subduction zone and at similar distances to the trench.

4.3 Impact structures

In the analysis of impact structures, morphological features are essential to infer aspects of the impact process. The diameter and the depth of the crater are interpreted in terms of the size of the impacting object and the impact velocity. The asymmetry of the crater is interpreted in terms of the impactor's shape and the obliquity of the impact angle (Littlefield and Dawson, 2006). Figure 6 shows our topographic analysis of

ESURFD
1, 387–405, 2013

Meteor Crater in Arizona, also known as Barringer Crater. It was formed by the impact of the Canyon Diablo iron meteorite about 50 000 yr ago in sedimentary rocks consisting predominantly of dolomites and minor sandstones (Barringer, 1905; Nishiizumi et al., 1991; Phillips et al., 1991). The crater shows a quadrangle shape and deviates from a circular or elliptical form due to preexisting joints. As such, a morphological analysis with simple topographic profiles is particularly difficult.

The baseline of our analysis follows the topographic high of the crater rim. About 4/5 of the entire crater contributes to the swath profile shown in Fig. 6b. Interestingly, the surface elevation declines uniformly at increasing distance to the rim (baseline) as indicated by a very low standard deviation ranging from 1 m at the floor to 13 m at the steepest faces.

5 Conclusions

We have extended the concept of swath profiles towards curved baselines allowing the analysis of river valleys, curved subduction zones, and crater rims. Our method directly uses the oriented distance of all surface points to the baseline. It immediately avoids artefacts of alternative ideas, namely the principal bias due to the curvature occurring in ordinary swath profiles and the non-uniform weighting of the surface points when stacking several individual profiles taken normal to the baseline. Furthermore, the new method is robust against the roughness of the baseline and can be implemented efficiently in a numerical code. The high efficiency even persists in case of surfaces consisting of unstructured point clouds instead of DEMs on a regular lattice. An implementation is available as an online tool (http://hergarten.at/geomorphology/swathprofile.php) and as a command line tool free of charge from the corresponding author.

ESURFD
1, 387–405, 2013

Title Page
Abstract Introduction
Conclusions References
Tables Figures
◀◀ ▶▶
◀ ▶
Back Close
Full Screen / Esc
Printer-friendly Version
Interactive Discussion

References

Barringer, D. M.: Coon Mountain and its crater, P. Acad. Nat. Sci. Phila., 57, 861–866, 1905. 397

Bonney, T. G.: Notes on the upper Engadine and the Italian valleys of Monte Rosa, and their relation to the glacier-erosion theory of lake-basins, Quarterly Journal of the Geological Society of London, 30, 479–489, 1874. 393

Bull, W. B.: Threshold of critical power in streams, Bull. Geol. Soc. Am., 90, 453–464, 1979. 393

Capitanio, F. A., Faccenna, C., Zlotnik, S., and Stegman, D. R.: Subduction dynamics and the origin of Andean orogeny and the Bolivian orocline, Nature, 480, 83–86, 2011. 395

Fielding, E., Isacks, B., Barazangi, M., and Duncan, C.: How flat is Tibet?, Geology, 22, 163–167, 1994. 389

Gephardt, J. W.: Topography and subduction geometry in the central Andes: Clues to the mechanics of a noncollisional orogen, J. Geophys. Res., 99, 12279–12288, 1994. 395

Gesch, D., Oimoen, M., Greenlee, S., Nelson, C., Steuck, M., and Tyler, D.: The National Elevation Dataset, Photogramm. Eng. Rem. S., 68, 5–11, 2002. 402

Grohmann, C. H.: Morphometric analysis in Geographic Information Systems: applications of free software GRASS and R, Comp. Geosci., 30, 1055–1067, 2004. 389

Gutenberg, B., Buwalda, J. P., and Sharp, R. P.: Seismic explorations on the floor of Yosemite Valley, California, Bull Geol. Soc. Am., 67, 1051–1078, 1956. 394

Isacks, B. L.: Uplift of the central Andean plateau and bending of the Bolivian orocline, J. Geophys. Res., 93, 3211–3231, doi:10.1029/JB093iB04p03211, 1988. 395

Littlefield, D. L. and Dawson, A.: The role of impactor shape and obliquity on crater evolution in celestial impacts, Int. J. Impact Eng., 33, 371–371, 2006. 396

Mitchell, S. G. and Montgomery, D. R.: Influence of a glacial buzzsaw on the height and morphology of the central Washington Cascade Range, USA, Quaternary Res., 65, 96–107, 2006a. 389

Mitchell, S. G. and Montgomery, D. R.: Polygenetic topography of the Cascade Range, Washington State, USA, Am. J. Sci., 306, 736–768, 2006b. 389

Montgomery, D. R.: Slope distributions, hillslope thresholds and steady-state topography, Am. J. Sci., 301, 432–454, 2001. 389

Nishiizumi, K., Kohl, C. P., Shoemaker, E. M., Arnold, J. R., Klein, J., Fink, D., and Middleton, R.: In situ 10Be-26Al exposure ages at Meteor Crater, Arizona, Geochim. Cosmochim. Ac., 55, 2699–2703, 1991. 397

Pederson, J. L., Anders, M. D., Rittenhour, T. M., Sharp, W. D., Gosse, J. C., and Karlstrom, K. E.: Using fill terraces to understand incision rates and evolution of the Colorado River in eastern Grand Canyon, Arizona, J. Geophys. Res., 111, F02003, doi:10.1029/2004JF000201, 2006. 394

Phillips, F. M., Zreda, M. G., Smith, S. S., Elmore, D., Kubik, P. W., Dorn, R. I., and Roddy, D. J.: Age and geomorphic history of Meteor Crater, Arizona, from cosmogenic 36Cl and 14C in rock varnish, Geochim. Cosmochim. Ac., 55, 2695–2698, 1991. 397

Rehak, K., Strecker, M. R., and Echtler, H. P.: Morphotectonic segmentation of an active forearc, 37°–41°S, Chile, Geomorphology, 94, 98–116, 2008. 389

Reiners, P. W., Ehlers, T. A., Mitchell, S. G., and Montgomery, D. R.: Coupled spatial variations in precipitation and long-term erosion rates across the Washington Cascades, Nature, 426, 645–647, 2003. 389

Robl, J., Hergarten, S., and Stüwe, K.: Morphological analysis of the drainage system in the Eastern Alps, Tectonophysics, 460, 263–277, 2008. 389

Telbisz, T., Kovács, G., Székely, B., and Karátson, D.: The method of swath analysis based on digital terrain models (in Hungarian), Földtani Közlöny, 142, 193–200, 2012. 389

Wernicke, B.: The California River and its role in carving Grand Canyon, Bull. Geol. Soc. Am., 123, 1288–1316, 2011. 394

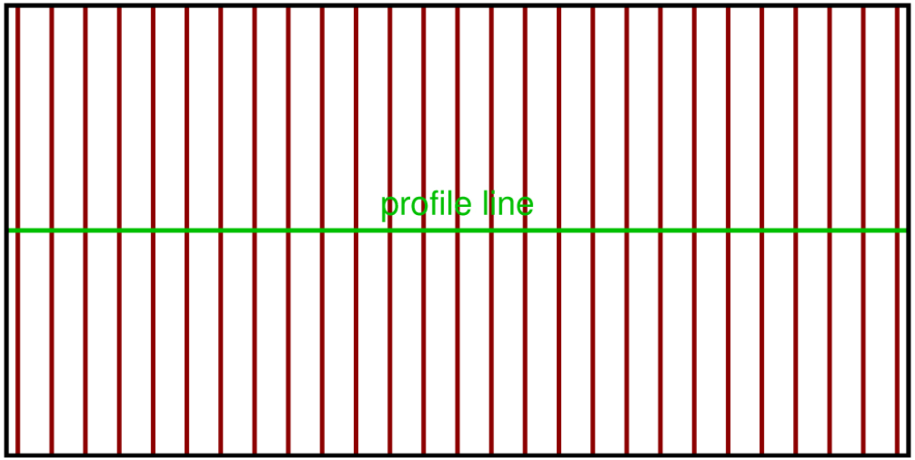

Fig. 1. Illustration of the idea of ordinary swath profiles. Green: profile line. Red: lines along which the elevation data are stacked.

ESURFD
1, 387–405, 2013

Generalized swath profiles

S. Hergarten et al.

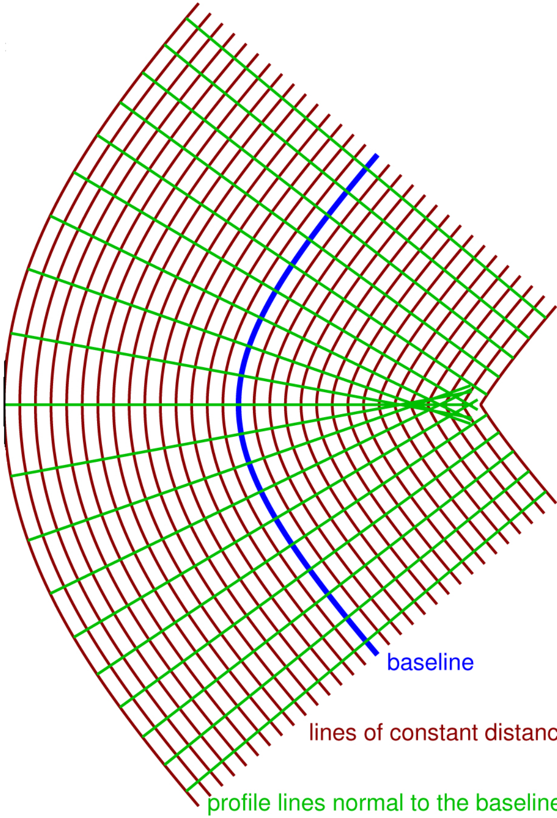

Fig. 2. Two ways of generalizing swath profiles towards curved baselines (blue). Green: profile lines normal to the baseline which might be stacked. Red: lines of constant oriented distance from the baseline (new method). The frame defines the region of all points which potentially contribute to the profile as discussed in Sect. 3.

ESURFD
1, 387–405, 2013

Generalized swath profiles

S. Hergarten et al.

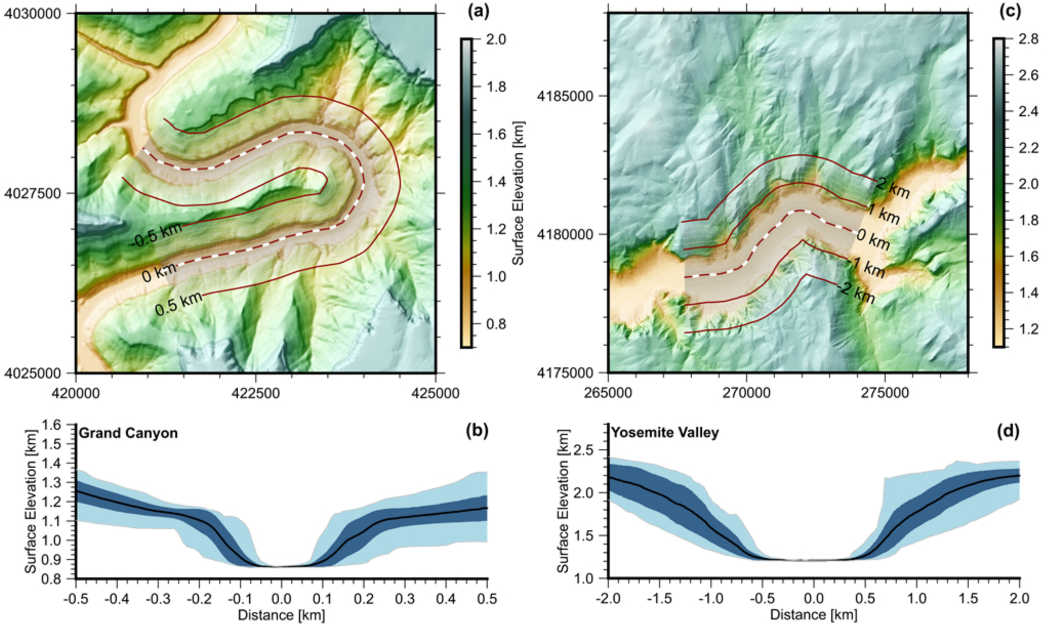

Fig. 3. Fluvially versus glacially coined valleys. The maps show sections of **(a)** the Grand Canyon drainage system formed by fluvial incision and **(c)** the Yosemite Valley coined by glacial scouring. The baseline and lines of constant oriented distance are indicated by red and white lines. The gray transparent region covers all values included in the swath profiles shown in **(b)** and **(d)**. Mean elevation (black line), extreme values (hull of the blue area) and mean elevation ±1 standard deviation (hull of the dark blue area) are plotted. Maps and swath profiles were derived from the National Elevation Dataset in the UTM coordinate system and a spatial resolution of 10 m (Gesch et al., 2002).

ESURFD

1, 387–405, 2013

Generalized swath profiles

S. Hergarten et al.

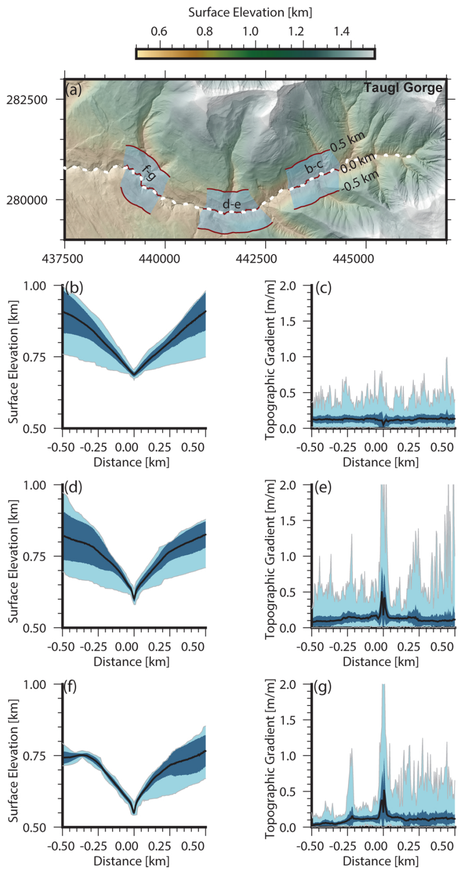

Fig. 4. Average geomorphic parameters of three morphologically different sections of the Taugl Gorge (Austria). The baseline (white dotted line) follows the course of the Taugl River. The blue transparent regions cover all values included in the profiles as annotated. Topography **(b, d, f)** and topographic gradient **(c, e, g)** are shown, comprising mean values (black line), extreme values (hull of the light blue area) and mean values ±1 standard deviation (hull of the dark area). Maps and profiles were derived from LiDAR based DEM data (spatial resolution 1 m) in the MGI Austria M31 coordinate system provided by the federal government of Salzburg.

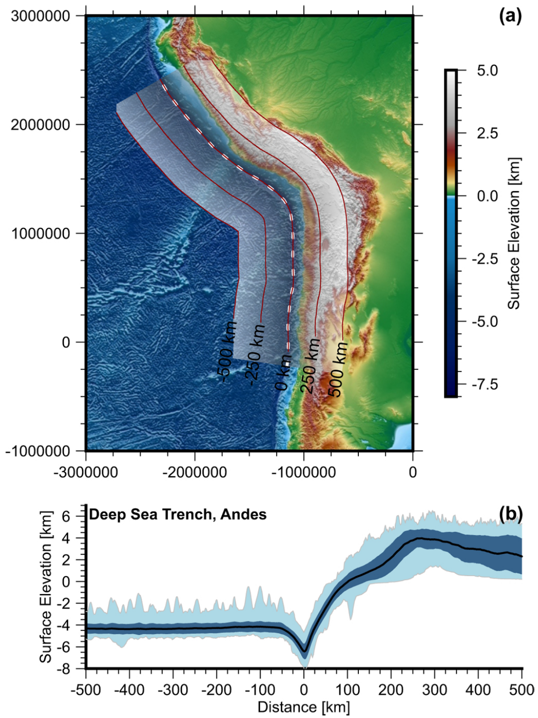

Fig. 5. Topographic and bathymetric representation of the converging Nazca and South American plate as an example of a curved subduction zone. The baseline of the generalized swath profile follows the trench (white dotted line). Red contours indicate the oriented distance to the baseline. The gray transparent region covers all values included in the profile. The mean elevation is shown by the black line. Extreme values and mean values ±1 standard deviation are indicated by the light- and dark blue areas, respectively. Map and profile were derived from the ETOPO1 digital elevation model (http://www.ngdc.noaa.gov/mgg/global/).

ESURFD
1, 387–405, 2013

Generalized swath profiles

S. Hergarten et al.

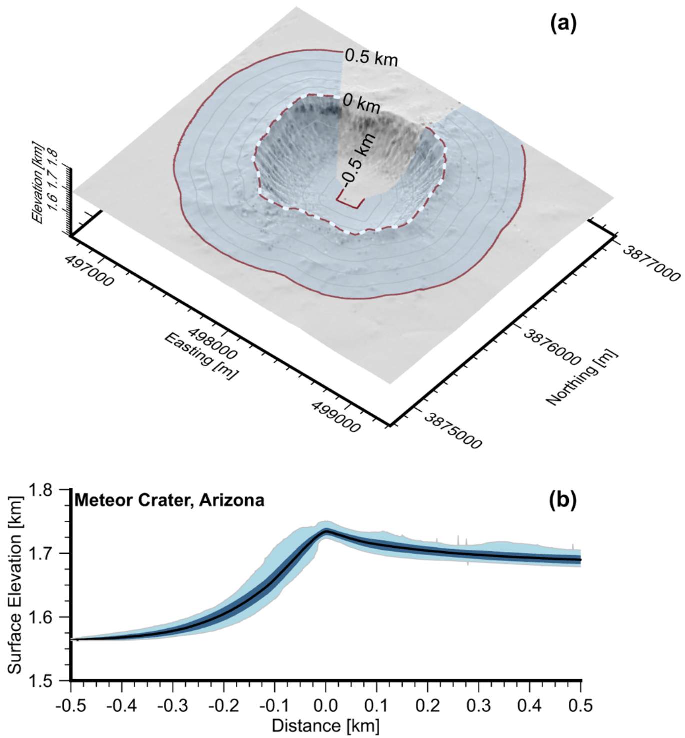

Fig. 6. Generalized swath profile analysis of Meteor Crater (Arizona). The baseline (white dotted line) follows the crater rim and contours indicate the horizontal distance to the baseline. The blue transparent region covers all values included in the profile. Mean elevation, (thick black line), extreme values (hull of the blue area), and mean elevation ±1 standard deviation (hull of the dark area) are shown. The map and the profile are based on the LiDAR point cloud processed by the National Center for Airborne Laser Mapping (http://www.ncalm.org) and interpolated onto a regular Cartesian grid (UTM coordinate system) with a spatial resolution of 2 m.

ESURFD
1, 387–405, 2013